NASA Technical Memorandum 110264
U. S. Army Research Laboratory Technical Report 1210

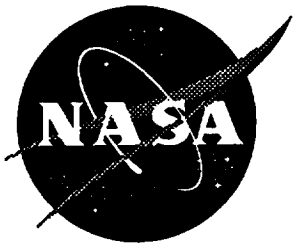

Evaluation of the Edge Crack Torsion (ECT) Test for Mode III Interlaminar Fracture Toughness of Laminated Composites

Jian Li
Langley Research Center, Hampton, Virginia

Shaw Ming Lee
Hexcel Composites, Anaheim, California

Edward W. Lee
Bell Helicopter Textron, Forth Worth, Texas

T. Kevin O'Brien
Vehicle Structures Directorate
U.S. Army Research Laboratory
Langley Research Center, Hampton, Virginia

August 1996

National Aeronautics and
Space Administration
Langley Research Center
Hampton, Virginia 23681-0001

ABSTRACT: An analytical and experimental investigation was carried out on G40-800/R6376 graphite epoxy laminates to evaluate the Edge Crack Torsion (ECT) test as a candidate for a standard Mode III interlaminar fracture toughness test for laminated composites. The ECT test consists of a $[90/(\pm 45)_3/(\mp 45)_3/90]_s$ laminate with a delamination introduced by a non-adhesive film at the mid-plane along one edge and loaded in a special fixture to create torsion along the length of the laminate. Dye penetrate enhanced X-radiograph of failed specimens revealed that the delamination initiated at the middle of the specimen length and propagated in a self similar manner along the laminate mid-plane. A three-dimensional finite element analysis was performed that indicated that a pure Mode III delamination exists at the middle of specimen length away from both ends. At the ends near the loading point a small Mode II component exists. However, the magnitude of this Mode II strain energy release rate at the loading point is small compared to the magnitude of Mode III component in the mid-section of the specimen. Hence, the ECT test yielded the desired Mode III delamination. The Mode III fracture toughness was obtained from a compliance calibration method and was in good agreement with the finite element results. Mode II End-Notched Flexure (ENF) tests and Mode I Double Cantilever Beam (DCB) tests were also performed for the same composite material. The Mode I fracture toughness was much smaller than both the Mode II and Mode III fracture toughness. The Mode II fracture toughness was found to be 75% of the Mode III fracture toughness.

KEY WORDS: composite materials, fracture toughness, delamination, compliance calibration, three-dimensional finite element analysis, strain energy release rate

Nomenclature

a delamination length for DCB and ENF specimens, m

$\tilde{a}$	delamination length for ECT specimens, m
Δa	virtual crack length, m
b	specimen width for DCB and ENF specimens, m
B	specimen width for ECT specimens, m
C	loading point compliance, $m \cdot N^{-1}$
δ	loading point displacement, m
δ_{xi}	relative crack face displacement in x-direction at node i and i', m
δ_{yi}	relative crack face displacement in y-direction at node i and i', m
δ_{zi}	relative crack face displacement in z-direction at node i and i', m
E_{ii}	Young's moduli, i=1, 2, 3, GPa
F_{xj}	nodal force in x-direction at node j
F_{yj}	nodal force in y-direction at node j
F_{zj}	nodal force in z-direction at node j
G_{ij}	shear moduli, ij=12, 13, 23, GPa
G	strain energy release rate, $J \cdot m^{-2}$
G_I	Mode I strain energy release rate component, $J \cdot m^{-2}$
G_{II}	Mode II strain energy release rate component, $J \cdot m^{-2}$
G_{III}	Mode III strain energy release rate component, $J \cdot m^{-2}$
G_{IC}	Mode I fracture toughness, $J \cdot m^{-2}$
G_{IIC}	Mode II fracture toughness, $J \cdot m^{-2}$
G_{IIIC}	Mode III fracture toughness, $kJ \cdot m^{-2}$
h	specimen thickness, m
H	ply thickness, m
L	effective ECT specimen length, m
L'	specimen length, m
2ℓ	span of ENF specimen, m

m	linear regression parameter for ECT tests
m'	linear regression parameter for ENF tests, $N^{-1} \cdot m^{-2}$
n	linear regression parameter for DCB tests
ν_{ij}	Poisson's ratio, ij=12, 13 and 23
P	transverse load, N
P_c	transverse load at delamination growth, N
W	moment arm length for ECT specimens, m
x, y, z	Cartesian coordinates

Introduction

Recently the Edge Crack Torsion (ECT) test was proposed as a candidate standard Mode III fracture toughness test for laminated composites [1]. The ECT test consists of a $[90/(\pm 45)_3/(\mp 45)_3/90]_s$ laminate with a delamination introduced by a non-adhesive film inserted at the mid-plane along one edge during manufacture and loaded in a special fixture to create torsion along the length of the laminate. Previous analytical investigations of the ECT test [2,3] indicated that the failure mode is Mode III in the portion of the specimen away from both ends where the load nose and supports contact the specimen. However, experimental evidence of Mode III delamination growth from the insert is needed to justify the validity of the ECT test. In addition, to understand the boundary effects, a full three-dimensional finite element analysis is required.

The first objective of this paper was to understand and document the nature of delamination growth in the ECT specimen. The second objective was to develop a three-dimensional finite element model of the ECT specimen to accurately evaluate the individual mode and total strain energy release rate along the delamination front, taking into account the three-dimensional effects neglected by previous analytical investigation [2,3]. To this end,

G40-800/R6376 graphite/epoxy laminates were manufactured by Ciba Composites and were tested monotonically to failure in the ECT fixture. A three-dimensional finite element analysis of a typical ECT specimen was also performed. To compare the magnitude of Mode III fracture toughness to the Mode II fracture toughness, Mode II tests were performed using End-Notched Flexture (ENF) specimens. In addition, Mode I Double Cantilever Beam (DCB) tests were also performed for a complete comparison. In the paper, the test results for the ECT specimens, the ENF specimens and the DCB specimens were presented first, followed by the three-dimensional finite element analysis of a typical specimen.

Experimental Investigation

Specimen Configuration

The ECT laminate specimen shown in Figure 1 was an 89 mm long (L') by 38 mm wide (B) (3.5 in. × 1.5 in.) rectangular plate, where the span (L) and the moment arm (W) were 76 mm (3 in.) and 32 mm (1.25 in.), respectively. The average specimen thickness (h) was 4.9 mm (0.193 in.). The ECT specimens were cut from a $[90/(\pm 45)_3/(\mp 45)_3/90]_s$ laminated panel with embedded 13 μm non-adhesive Polytetrafluoroethylene (PTFE) films embedded at the mid-plane along one edge to introduce an edge delamination crack of length, ã. The panel was made of G40-800/R6376 graphite/epoxy tape plies. The fiber aerial weight (FAW) and fiber density (FD) were 190 $g \cdot m^{-2}$ and 1.80 $g \cdot cm^{-3}$, respectively. The fiber volume fraction (V_f) for the ECT specimens was calculated to be 60 %, (percent V_f=(Number of plies)·(FAW)/[h·(FD)]·100). C-scans were used to determine the insert location in the panel which helped when cutting the panel into specimens. Due to the unstable delamination growth of the ECT specimen [1], a series of specimens with initial delamination lengths varying between 0 to 19 mm (0.75 in.) were made to generate a compliance calibration curve. Three groups of specimens, with six replicates each, were cut from a single panel. Within each group, the insert lengths (initial delamination lengths, ã) were 0, 2.5, 5, 11, 16 and 19 mm, respectively. Note the delamination length ã was measured from the free edge to the end of

insert while the delamination length, a, was measured from the loadline to the end of insert for both DCB and ENF specimens.

Experimental Procedure

The ECT specimen was placed in the ECT test fixture shown in Figure 2. The fixture provided supports at three points, and the transverse load was introduced at the fourth point by compression of the loading pin. The loading pin was loaded in the test machine with a constant stroke rate of 1.5 mm·min^{-1}. During the test, the specimen was subjected to end torsion induced by a pair of counteracting moments at a distance L=76 mm (3 in.) apart. Each moment was generated by a pair of forces with a moment arm W=32 mm (1.25 in.). The applied load P versus load-point displacement δ was recorded on an X-Y plotter for each specimen.

Test Results

A typical load-displacement (P-δ) curve was shown in Figure 3. The curve was nearly linear up to the point A. After this point, the delamination grew from the insert and the stiffness decreased until a load drop was observed at P_c. A line tangent to the initial linear portion of the loading curve was drawn to determine the initial compliance $C=\delta/P$. Initial deviation from linearity due to seating of the loading fixture was ignored. The critical load for delamination propagation was defined as P_c. The critical load P_c along with the initial delamination length was used to calculate the critical total strain energy release rate G_c.

Dye penetrate enhanced X-radiographs of the ECT specimens, taken after the load drop occurred, were used to identify the delamination growth from the insert. Figures 4 (a) and (b) showed two different shapes of the delamination front for specimens with insert widths of 11 mm and 2.5 mm, respectively. In Figure 4 (a), the delamination initiated at the end of the insert in the middle of the effective specimen length and propagated in a self similar manner along the laminate mid-plane between the two 90° plies. Hence, the desired Mode III delamination

growth pattern was achieved in this specimen.

However, for the specimen with the 2.5 mm insert, shown in Figure 4 (b), the delamination grew off center of the effective specimen length. An examination of the edge of the specimen indicated that delaminations grew at the 90/45 and the 45/-45 interfaces. No delamination growth was evident between the two mid-plane 90° plies where the insert was placed. Thus Mode III type delamination growth was not achieved in this specimen. This behavior could be attributed to the fact that the insert length was too small. As observed in Ref. 2, the strain energy release rate dropped sharply from a plateau value to zero as the normalized initial delamination length ($\tilde{a}$/B) reduced from about 20% to zero under the same twist. In Figure 4(b) the normalized initial delamination length was ($\tilde{a}$/B)=0.07. This value appears to be too small to have enough delamination driving force at the insert front to initiate Mode III type delamination growth. Consequently, specimens with insert length of 2.5 and 5 mm were discarded.

Mode III-Compliance Calibration Method

When the critical strain energy release rate is established experimentally from measuring the change in compliance of the cracked body as a function of crack length, the data reduction method is usually referred to as the compliance calibration method. As shown in Ref. 4, the strain energy release rate can be calculated from the change of compliance with crack length of the delaminated specimen as

$$G = \frac{P^2}{2L}\frac{\partial C}{\partial \tilde{a}} \tag{1}$$

where $\frac{\partial C}{\partial \tilde{a}}$ is the rate of change in compliance as the crack grows.

Two procedures are often adopted in the experimental evaluation to approximate the derivative of C with respective to ã. In the first procedure, the delamination is extended by a small increment $\Delta\tilde{a}$ and the change in compliance ΔC is measured. Then the ratio $(\Delta C/\Delta\tilde{a})$ is used to approximate the derivative in Equation 1. In the second procedure, the compliance C is measured by varying the initial crack length ã by moving the specimen in the test fixture and applying a small load to establish the specimen compliance without growing the crack. A plot of C versus ã is then generated. A least squares curve fit is applied to determine C as a function of crack length. The derivative of compliance as a function of ã can then be substituted into Equation 1.

Unfortunately, for the ECT configuration it is not possible to generate a compliance curve from a single ECT specimen using either method because of (1) the unstable delamination growth and (2) it is not possible to shift the specimen in the fixture and change the initial delamination length, ã. Hence, a number of specimens with different insert lengths were tested to obtained a plot of compliance as a function of delamination length. First, the 1/C (the inverse of compliance) values were plotted as a function of normalized delamination length ã/B as shown in Figure 5. Then, a least square straight line fit to the data was determined. The linear relationship between (1/C) and (ã/B) represented by the straight line can be expressed as

$$\frac{1}{C} = A\left[1 - m\left(\frac{\tilde{a}}{B}\right)\right] \tag{2}$$

where m and A are constants. The Mode III fracture toughness, G_{IIIc}, can be obtained by differentiating Equation (2) with respect to delamination length ã and substituting the derivative of C with respect to ã into Equation (1), yielding

$$G_{IIIc} = \frac{mP_c^2C}{2LB\left[1 - m\left(\frac{\tilde{a}}{B}\right)\right]} \quad . \tag{3}$$

For the data presented in Figure 5, m and A were obtained as 0.9 and 415 $kN \cdot m^{-1}$. The Mode III fracture toughness G_{IIIc} of the individual specimens can be calculated using measured values of C and P_c from the individual specimens and the value of m from the curve fit described above. The critical load P_c, the inverse of the compliance 1/C, and the fracture toughness were presented in Table 1 along with the specimen thickness and initial delamination length. A more accurate delamination length measurement was made after the test by completely opening the delamination and observing the delamination surfaces. The end of the insert could be readily distinguished from the propagated delamination on the delaminated surfaces. For specimens where the insert front was not straight, the delamination length was determined from the average of the insert length measurements at 6 or more equally spaced locations along the insert front. If these measurements showed large variations, the results should be discarded. Specimens with insert lengths measured as 11 mm, 16 mm and 19 mm before the test were opened after the test. The insert front was fairly straight in these specimens (within 1 mm) and hence no results were discarded. The measured insert length after the test was within 1 mm of the initial measurement for each of these specimens. For the nine G40-800/R6376 graphite epoxy specimens tested, the mean Mode III fracture toughness, G_{IIIc}, was 1419 $J \cdot m^{-2}$ with a coefficient of variation of 8.2%.

Comparison with Other Delamination Fracture Modes

Mode II Fracture Toughness

In order to compare the Mode III fracture toughness to the Mode II fracture toughness of the G40-800/R6367 graphite epoxy material, End-Notched Flexure (ENF) Mode II tests [5,6] were also performed. The ENF specimen configuration, shown in Figure 6 (a), consisted

of a unidirectional laminate with a mid-plane embedded insert at one end subjected to 3-point bending loading. The total specimen length was about 250 mm, width b was 25 mm and the thickness h was 4.3 mm (24 unidirectional plies). The length between the two supports (2ℓ) is 100 mm. A 13 μm non-adhesive PTFE film was placed at the laminate mid-plane during manufacture. The insert length was 60 mm for each specimen. The ENF apparatus is shown in Figure 6 (b) where a spring-loaded displacement gauge is mounted under the specimen as shown.

The specimens were loaded and unloaded in the elastic range first to obtain compliance with respect to initial delamination lengths of a=0, 15, 20, 25, 30, 35, and 40 mm. This was achieved by keeping the supports fixed and sliding the specimen in the rig to achieve different initial delamination lengths. Note that sliding the specimen produced different distances between the right roller support and the tip of the insert (a in Figure 6(a)). Specimens were loaded in displacement control loading with a constant stroke rate of 0.5 mm/min. After the compliance measurements, a least squares linear regression of the following form was performed,

$$C = C_0 + m' a^3 \tag{4}$$

The results of the compliance calibration tests for each specimen were presented in Table 2 along with the corresponding value of m'.

The specimen was then positioned in the test fixture so that a/ℓ=0.5, and loaded until the delamination started to grow from the insert. The Mode II fracture toughness was evaluated based on the compliance calibration [6] as

$$G_{IIc} = \frac{3m' a^2 P_c^2}{2b} \tag{5}$$

The maximum load and the initial delamination length was used in Equation 5 to calculate G_{IIc}. A total of five specimens were tested. The test results were presented in Table 3. One specimen was completely separated after the test to verify the insert length. The mean Mode II fracture toughness G_{IIC} was 1061 $J \cdot m^{-2}$ with a coefficient of variation of 9.8%. This value of Mode II fracture toughness was 75% of the Mode III fracture toughness for this material.

Mode I Fracture Toughness

For a complete comparison, Mode I Double Cantilever Beam (DCB) tests were also performed in a manner largely following the ASTM Test Method for Mode I Interlaminar Fracture Toughness of Unidirectional Fiber-Reinforced Polymer Matrix Composites (D 5528-94a). A 13 μm thick non-adhesive PTFE film was placed in the mid-plane of the laminate during fabrication to introduce initial delamination to the specimens that were subsequently cut from the laminate. The DCB test specimens were 4.3 mm thick (h) (24 ply unidirectional laminate), 12.5 mm wide (b) and 190 mm long (L'). The 0° fibers were oriented along the length of the specimens. A schematic of the DCB specimen was shown in Figure 7. For each specimen, the insert length was about 45 mm from the specimen end or 38 mm from the load line. To introduce load to the specimen, loading blocks of 13 mm x 13 mm x 13 mm were bonded to the specimen end using an adhesive. A total of five specimens were tested.

The DCB specimens were loaded in a test machine at a displacement rate of 0.5 $mm \cdot min^{-1}$ to open and propagate the cracks. The specimen edges were painted with a white typewriter correction fluid to help identify the delamination front during the tests. Initial delamination growth from the insert for each specimen was determined from the sudden load drop of the initial linear load-displacement trace. As the delamination grew further, the location of the crack front was marked on the specimen edge at a crack growth interval of about 6 mm.

For each marked crack front, the corresponding location on the load-displacement trace was also recorded for later data reduction.

To calculate the Mode I fracture toughness, G_{IC}, the compliance calibration method was used for data reduction [7]. A least squares fit of the log-log plot of specimen compliance $C=\delta/P$ as a function of delamination length was performed to obtain a slop n where $C=K\cdot a^n$ (where K is a constant). The Mode I fracture toughness G_{IC} was determined from,

$$G_{IC} = \frac{nP\delta}{2ba} \tag{6}$$

The initial G_{IC} values were calculated from n along with the P, δ and a values associated with the delamination onset from the insert. These G_{IC} values and the n value obtained were given in Table 4. The average initial G_{IC} value was 322 $J\cdot m^{-2}$ with a coefficient of variation of 7.6%.

The comparison of various modes of fracture toughness from the DCB, ENF and ECT tests was shown in Figure 8. The DCB Mode I fracture toughness was about 30% of the ENF Mode II fracture toughness and 23% of the ECT Mode III fracture toughness for the G40-800/R6376 graphite epoxy studied.

Analytical Investigation

Finite Element Model

A finite element model for ECT specimen C5 in Table 1 with dimensions $89\times38\times4.8$ mm ($3.5\times1.5\times0.189$ in.) was developed using 34,048 eight-node solid elements (SOLID45). The ANSYS finite element analysis software package (Version 5.1) was used for the analysis. A finite element mesh of the ECT specimen is shown in Figure 9 along with a cross section view of the detailed finite element mesh at the delamination front and an enlarged view of the

mesh at a specimen corner. Each ply thickness (H) was assumed to be 0.171 mm (0.00675 in.). The initial crack length of 19 mm (0.75 in.) was assumed. The crack plane was modeled with double nodes of zero distance connected by 4669 frictionless point-to-surface contact elements (CONTAC49) to prevent interpenetration of the two delamination surfaces. The specimen length was modeled with 28 equally spaced elements. The specimen width was modeled with 38 elements distributed symmetrically about the half width. The element size at the half width where the crack tip was located was 0.171 mm (0.00675 in.), and increased linearly to 3.175 mm (0.125 in.) at the two edges. The thickness of each ply was modeled by one element except for the two 90° plies on either side of the mid-plane. These plies were each modeled with three equal sized elements through-the-thickness. Therefore the mesh size of the elements surrounding the delamination crack tip was 1/3H×H (see Figure 9b).

The lamina elastic properties were obtained from tension tests of unidirectional and ±45° laminate coupons and were presented in Table 5. In the analysis, $G_{23} = G_{12}$ and $\nu_{23} = \nu_{12}$ were assumed because G_{23} or ν_{23} are much more difficult to determine experimentally. According to the analyses presented in reference 2, these assumptions result in conservative estimation of the critical strain energy release rate compared with other G_{23} values ($0 \le G_{23} < G_{12}$). The effect of these assumptions on the prediction of the strain energy release rate components were studied by the present three-dimensional finite element model and the results were presented in the Appendix. As shown in the Appendix the assumptions of $G_{23} = G_{12}$ and $\nu_{23} = \nu_{12}$ resulted in slightly lower Mode III strain energy release rate component than the case where $G_{23}=V_f G_{12}$ and $\nu_{23}=(E_{22}/2G_{23}-1)$ were used. For G_{23} values differing by 40%, the differences in the average total strain energy release rate and Mode III component were 9% and 10%. The effect of G_{23} and ν_{23} on the strain energy release rate values may be considered small. The three-dimensional finite element analysis confirmed the two-dimensional analytical predictions on the G_{23} effect on strain energy release rate.

The model was supported in z-direction at three nodes where the nodal locations were equivalent to the position of the three supporting pins on the ECT test fixture. The remaining two translational rigid body motions were also prevented by constraining the degree of freedoms along x-direction and y-direction at two of these supporting nodes. A critical test load of 1045 N (235 pounds) for specimen C5 (corresponding to a load point displacement of 4.63 mm) was applied at a node that was located 3.175 mm (0.125 inch) along the specimen length, and 3.175 mm (0.125 inch) in from the edge, from the specimen corner. Because the ECT model contained contact elements, the analysis required a geometrically nonlinear solution to update the deformed geometry during the solution process. However, contact was only found in the local vicinity near the loading points as shown in Figure 10, and hence, did not influence the calculated strain energy release rate components.

Virtual Crack Closure Technique

The virtual-crack-closure-technique (VCCT) [7] was used to calculate the strain energy release rate components for Mode I, Mode II and Mode III. The VCCT uses the stresses/nodal forces ahead of the delamination front and the displacements behind the front to determine the G components. A simple formula for calculating the strain energy release rate components for two-dimensional four-node elements was given by Rybicki and Kanninen [8]. This formula uses the forces at the crack tip and the relative displacements of the crack faces behind the crack tip to calculate the G components. The strain energy release rate components can be calculated from the work required to close the delamination by one element length Δa (see Figure 11 (a)) as

$$G_I = \frac{F_{zj}\delta_{zi}}{2\Delta a} \tag{7}$$

$$G_{II} = \frac{F_{yj}\delta_{yi}}{2\Delta a} \tag{8}$$

where F_{yj} and F_{zj} are the forces in the y-direction and z-direction at node j, δ_{yi} and δ_{zi} are the relative crack face displacements between nodes i and i', located at a distance Δa behind the crack tip in the y-direction and z-direction, respectively.

Extension of these formulas to three-dimensional eight-node solid elements is straight forward. The strain energy release rate components are calculated (see Figure 11 (b)) from

$$G_I = \frac{F_{zj}\delta_{zi}}{2\Delta a \Delta x} \tag{9}$$

$$G_{II} = \frac{F_{yj}\delta_{yi}}{2\Delta a \Delta x} \tag{10}$$

$$G_{III} = \frac{F_{xj}\delta_{xi}}{2\Delta a \Delta x} \tag{11}$$

where Δx is the sum of one-half the element lengths on either side of node j in the x-direction.

Numerical Results

The typical distribution of strain energy release rate components along the length of the delamination front was shown in Figure 12. The Mode I component was negligibly small along the entire delamination front. A finite Mode II component was observed near the loading points, but diminished away from the loading point. The Mode III component raised from zero at both ends and reached a plateau about 20% into the specimen length from either support. The plateau value of the Mode III component was much higher (by a factor nearly equal to 3) than the maximum Mode II value observed at the loading point. Note that the Mode II fracture toughness was about 75% of the fracture toughness from the ECT tests in previous section, hence, the magnitude of the Mode II component at the loading point will not reach the Mode II

fracture toughness when the magnitude of Mode III component in the mid-section of the specimen reaches the Mode III fracture toughness. Hence, a Mode III delamination will initiate in the ECT specimen.

The three-dimensional finite element analysis shows that the delamination will grow in pure Mode III at the middle of the specimen length away from both ends. This is in agreement with the experimental observation from the dye penetrate enhanced X-radiograph shown in Figure 4 (a). An average strain energy release rate component can be calculated by integrating that component over the effective region along the delamination front and then divided by the effective length of the ECT specimen. The average total strain energy release rate and the Mode III component computed from the finite element model were 1349 $J \cdot m^{-2}$ and 1239 $J \cdot m^{-2}$, respectively, which indicated the critical total strain energy release rate integrated along the delamination front was 92% Mode III. The critical total strain energy release rate for the ECT specimen can be used to approximate the Mode III fracture toughness. The finite element result for the average total strain energy release rate agreed very well with the mean test result of 1419 $J \cdot m^{-2}$ determined using compliance calibration.

Concluding Remarks

An analytical and experimental investigation was carried out on G40-800/R6376 graphite epoxy laminates to evaluate the Edge Crack Torsion (ECT) test as a candidate standard Mode III interlaminar fracture toughness test for laminated composites. Dye penetrate enhanced X-radiographs of failed specimens revealed that the delamination initiated at the middle of the specimen length and propagated in a self similar manner in the laminate mid-plane. A three-dimensional finite element analysis was performed that indicated that a pure Mode III delamination will exist at the middle of specimen length away from both ends. A Mode II component was also shown to exist near the ends where the loading points are located. However, the magnitude of the Mode II strain energy release rate at the loading point was

much smaller than the magnitude of Mode III component in the mid-section of the specimen. Hence, the failure mode was the anticipated Mode III delamination. The total strain energy release rate calculated from the finite element model, with the applied load (P) equaled the critical load (P_c) observed in the experiment, was in good agreement with the fracture toughness evaluated from the compliance calibration method for the ECT specimen. The mean Mode III fracture toughness from nine specimens was 1419 $J \cdot m^{-2}$ with a coefficient of variation of 8.2%. Mode I DCB and Mode II ENF tests were also performed on the same composite material. The mean Mode II fracture toughness from five specimens was found to be 75% of the ECT Mode III fracture toughness. The average Mode I fracture toughness from five DCB specimens was about 30% of the ENF Mode II fracture toughness and 23% of the ECT Mode III fracture toughness.

Acknowledgment

This work was performed while the first author was a National Research Council Research Associate with the Army Research Laboratory Vehicle Structures Directorate at NASA Langley Research Center.

Appendix

Shear Modulus G_{23} Effect on the Calculation of Strain Energy Release Rate

The purpose of this appendix was to study the effect of G_{23} and ν_{23} on the strain energy release rate components for the ECT specimen under consideration. The three-dimensional finite element model for specimen C5 shown in Figure 9 was re-analyzed under the same loading conditions with the material properties $G_{23}=V_f \cdot G_{12}=2.91$ GPa and $\nu_{23}=(E_{22}/2G_{23}-1)=0.54$ while retaining the other material properties in Table 5. The distributions of the strain energy release rate components along the delamination front were plotted in Figure 13 along with the results shown in Figure 12 for comparisons. Case 1 represents the results from the three-dimensional finite element analysis by using the

assumptions of $G_{23}=G_{12}=5.15$ GPa and $\nu_{23}=\nu_{12}=0.325$ while case 2 represents the result with the properties $G_{23}=2.91$ GPa and $\nu_{23}=0.54$. Figure 13 shows that the distributions of the individual mode strain energy release rate are similar for these two cases. The Mode III component was higher for case 2 than case 1 by about 10%. The Mode II component was nearly the same throughout the effective length of the ECT specimen in both cases except at the loading and support locations where it was lower in case 2 than in case 1. The average total strain energy release rate and Mode III component for both cases are summarized in the following table:

	Average Strain Energy Release Rate $J \cdot m^{-2}$	
	Total	Mode III
Case 1	1349	1239
Case 2	1480	1371

The average total strain energy release rate and Mode III strain energy release rate component obtained from the two cases differed by about nine and ten percent for G_{23} values differing by 40%. Hence the effect of G_{23} and ν_{23} on the strain energy release rate calculation appears to be small. The assumptions on G_{23} and ν_{23} in case 1 give conservative predictions on the total strain energy release rate and the Mode III component. These observations are in agreement with the two-dimensional analytical predictions given in reference 2.

References

[1] Lee, S. M., "An Edge Crack Torsion Method for Mode III Delamination Fracture Testing," *Journal of Composite Technology & Research*, Vol. 15, No. 3, Fall 1993, pp. 193-201.

[2] Li, J. and O'Brien, T. K., "Simplified Data Reduction Methods for the ECT Test for Mode III Interlaminar Fracture Toughness," *Journal of Composites Technology and Research*, Vol. 18, No. 1, April, 1996, pp. 96-101.

[3] Li, J. and O'Brien, T. K. "Analytical Investigation of the Hygrothermal Effects and Parametric Study of the Edge Crack Torsion (ECT) Mode III Test Lay-ups," NASA TM 110183 June 1995 (also to appear in *Composite Materials: Fatigue and Fracture, Sixth Volume, ASTM STP 1285*).

[4] Irwin, G. R., "Structural Aspect of Brittle Fracture," *Applied Materials Research*, 3, pp. 65-81, 1964.

[5] Russell, A. J., "On the Measurement of Mode II Interlaminar Energies," DREP Materials Report 82-0, Defense Research Establishment Pacific, Victoria, BC, 1982.

[6] O'Brien, T. K., Murri, G. B. and Salpekar, S. A., "Interlaminar Shear Fracture Toughness and Fatigue Thresholds for Composite Materials," *Composite Materials: Fatigue and Fracture, Second Volume, ASTM STP 1012*, April, 1989, pp. 222-250.

[7] Irwin, G. R., "Analysis of Stresses and Strains near the End of a Crack Traversing a Plate," *Engineering Journal of Applied Mechanics*, Vol. 24, pp. 361-364, 1957.

[8] Rybicki, E. F. and Kanninan, M. F., "A Finite Element Calculation of Stress Intensity Factors by a Modified Crack-Closure Integral," *Engineering Fracture Mechanics*, Vol. 9, pp. 931-938, 1977.

Table 1. Test Results of the ECT Specimens

Specimen No.	Thickness (mm)	$\tilde{a}^*$ (mm)	1/C (kN·m^{-1})	P_c (N)	G_{IIIc} (J·m^{-2})
A3	5.1	11	347	1535	1411
A4	5.0	16	267	1165	1253
A5	4.7	19	226	1045	1341
B3	4.9	11	316	1432	1352
B4	4.8	16	267	1343	1657
B5	4.8	19	211	1050	1448
C3	5.0	11	317	1459	1397
C4	4.9	16	270	1236	1389
C5	4.8	19	200	1045	1519

*Specimens with 2.5 and 5 mm delamination lengths were discarded.

Table 2. Compliance Calibration Tests Results for ENF Specimens

	Compliance C for Specimen 1-5 (m·N^{-1} × 10^{-6})				
a (mm)	1	2	3	4	5
0	1.171	1.219	1.256	1.142	1.199
15	1.271	1.285	1.328	1.179	1.262
20	1.313	1.342	1.428	1.291	1.319
25	1.385	1.442	1.542	1.371	1.419
30	1.542	1.613	1.727	1.536	1.548
35	1.799	1.856	1.970	1.767	1.797
40	2.018	2.150	2.322	2.048	2.087
C_0	1.198	1.225	1.277	1.151	1.204
m' [N^{-1}·m^{-2}]	131.1	145.1	163.6	141.7	137.1

Table 3. Test Results of the ENF Specimens

Specimen No.	Thickness (mm)	δ_c (mm)	P_c (N)	G_{IIc} (J·m^{-2})
1	4.4	2.223	1557	1172
2	4.3	2.051	1379	1018
3	4.3	2.140	1374	1143
4	4.4	2.000	1423	1061
5	4.3	2.096	1343	912

Table 4 G_{IC} Results Obtained from DCB Tests Using Compliance Calibration Method ($C=K\cdot a^n$, $n=2.744$, $G_{IC} = n\cdot P\cdot\delta/(2\cdot b\cdot a)$)

Specimen No.	a, Crack Length (mm)	P, Load (N)	δ, Displacement (mm)	G_{IC} (J·m^{-2})
1	37.8	43.9	2.36	296
2	37.1	47.9	2.44	340
3	38.3	42.1	2.44	289
4	37.4	46.2	2.51	335
5	37.9	51.7	2.36	349

Table 5. Elastic properties of G40-800/R6376 graphite epoxy composite laminate

Properties
E_{11} = 151 GPa
$E_{22} = E_{33}$ =8.97 GPa
$G_{12} = G_{13}$ =5.15 GPa
$\nu_{12} = \nu_{13}$ =0.325

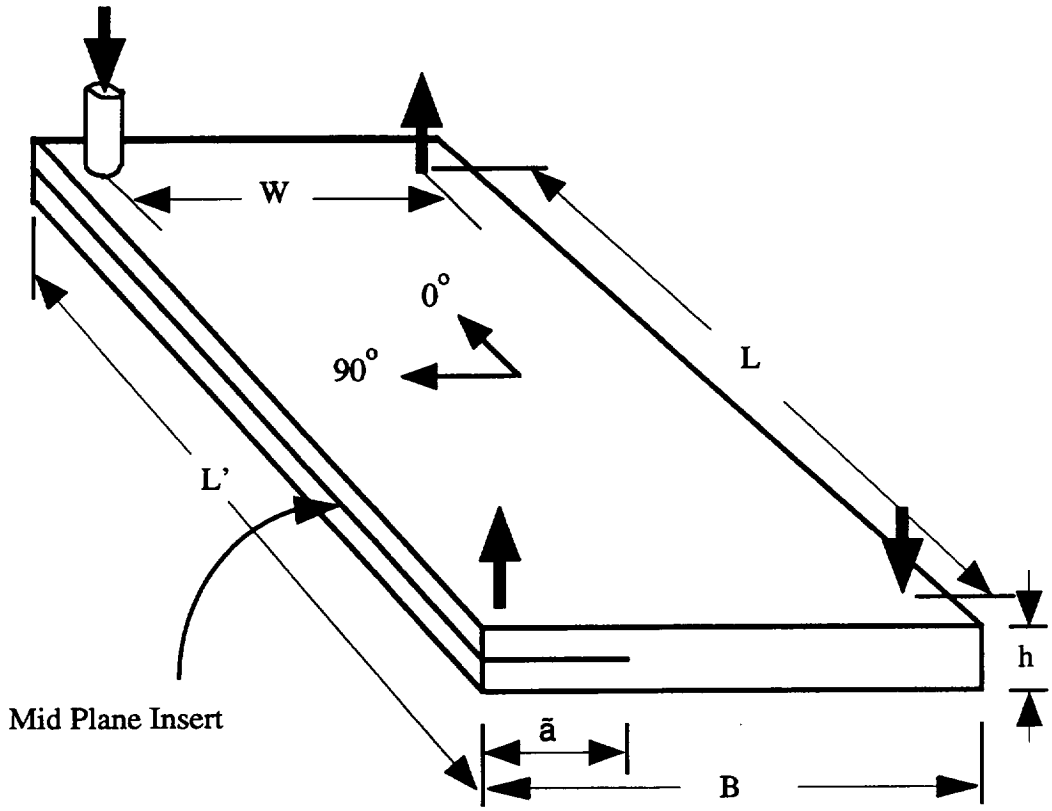

Figure 1. ECT specimen with an edge delamination introduced by a film insert.

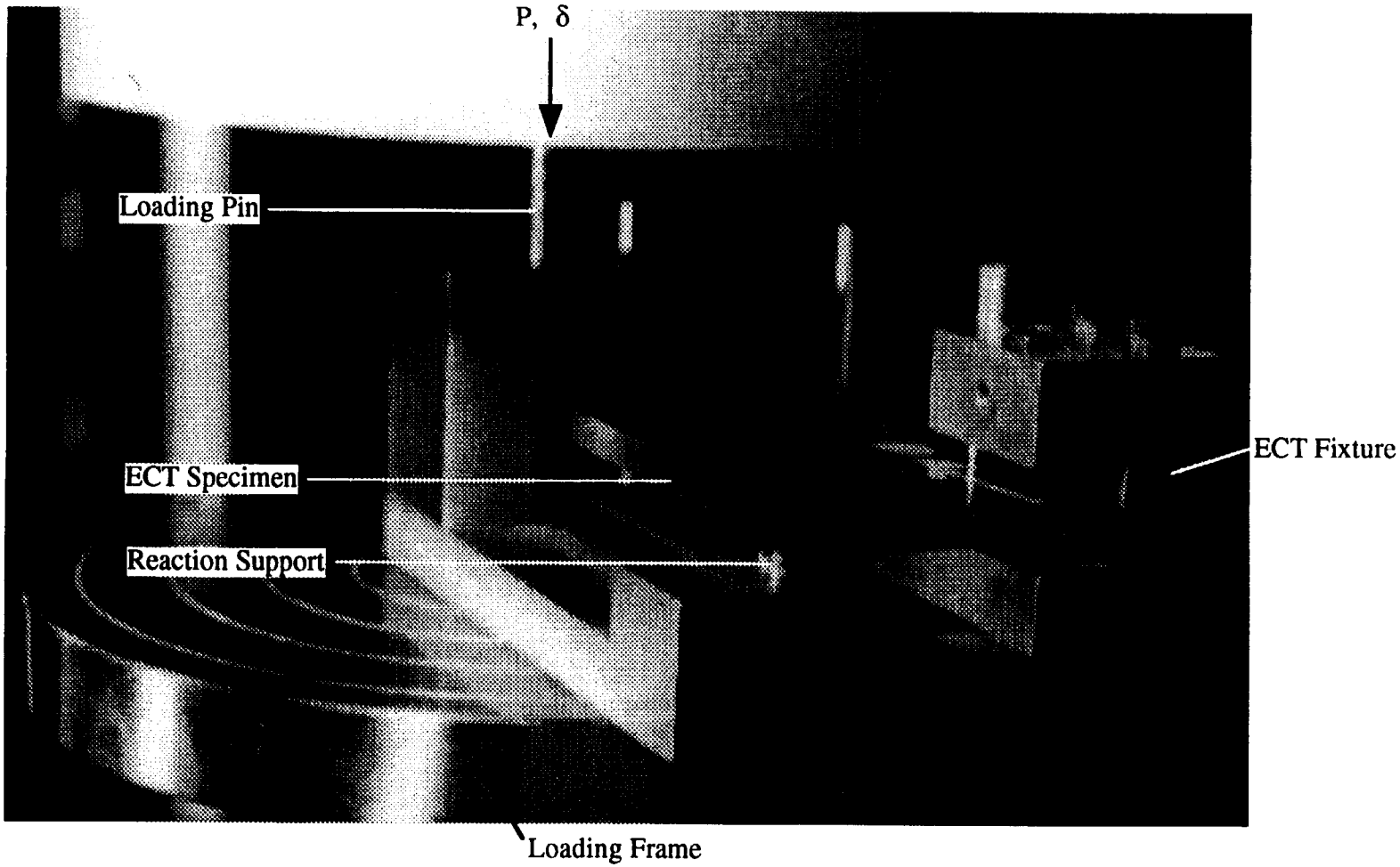

Figure 2. An ECT Specimen in the ECT fixture with load P and displacement δ applied to the loading pin.

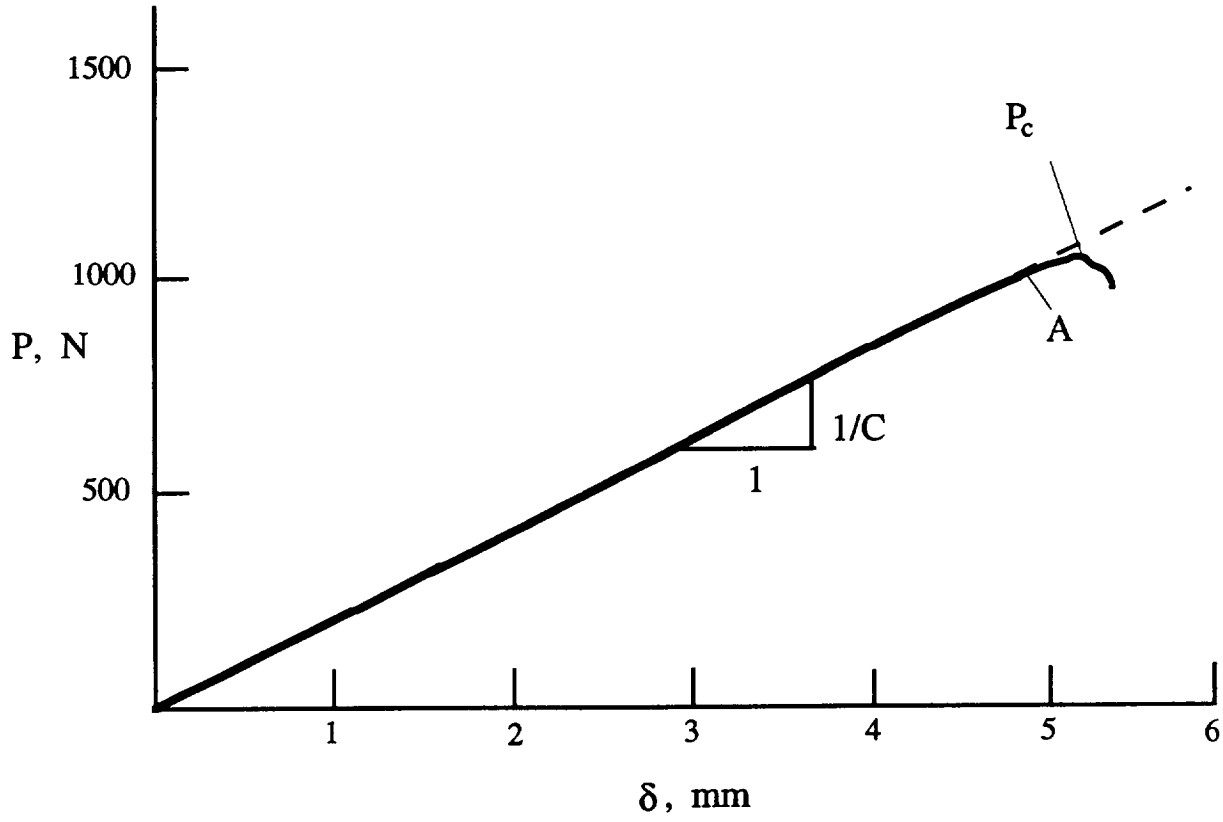

Figure 3. Compliance, C, and critical load, P_c, for the delamination onset determined from the ECT P-δ curve.

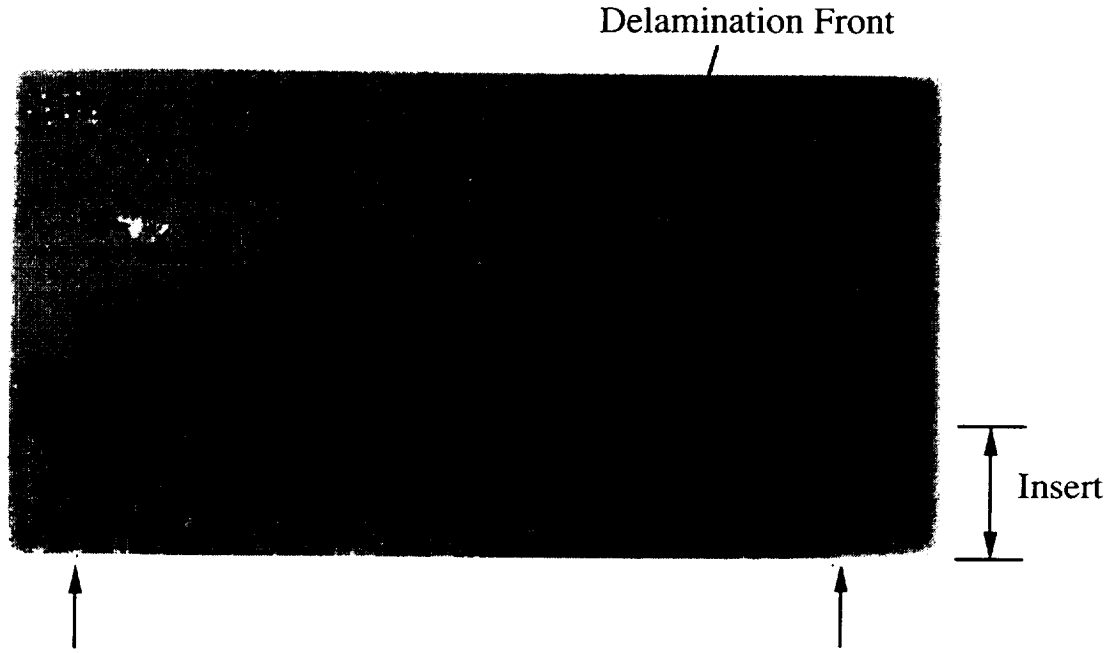

(a) Insert Length of 11 mm

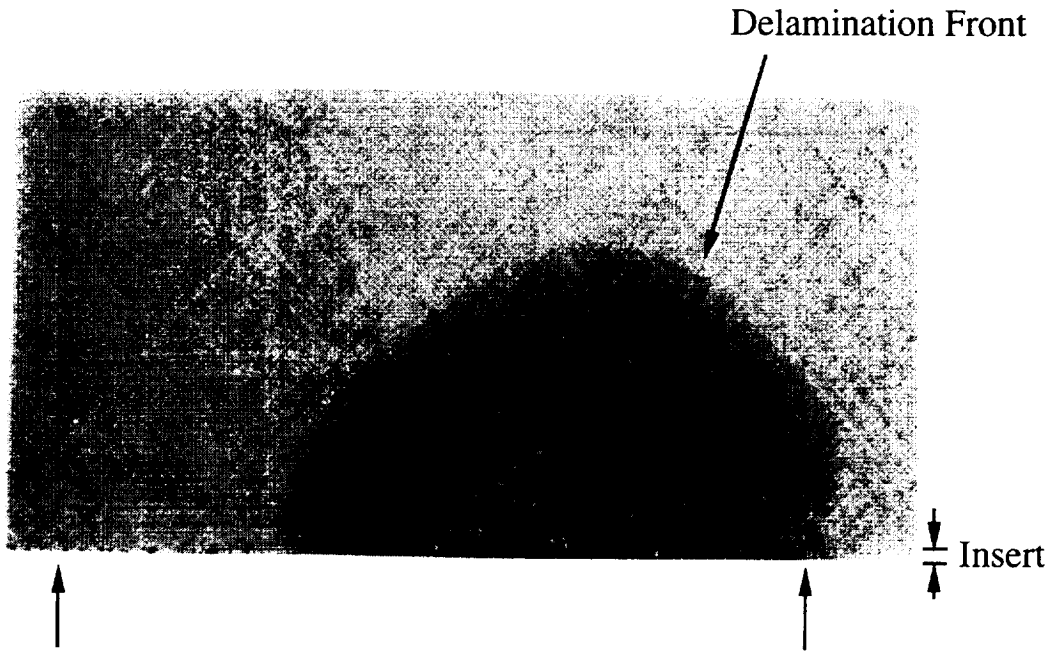

(b) Insert Length of 2.5 mm

Figure 4. Dye penetrate enhanced X-radiographs of failed ECT specimens for insert lengths of 11 mm and 2.5 mm.

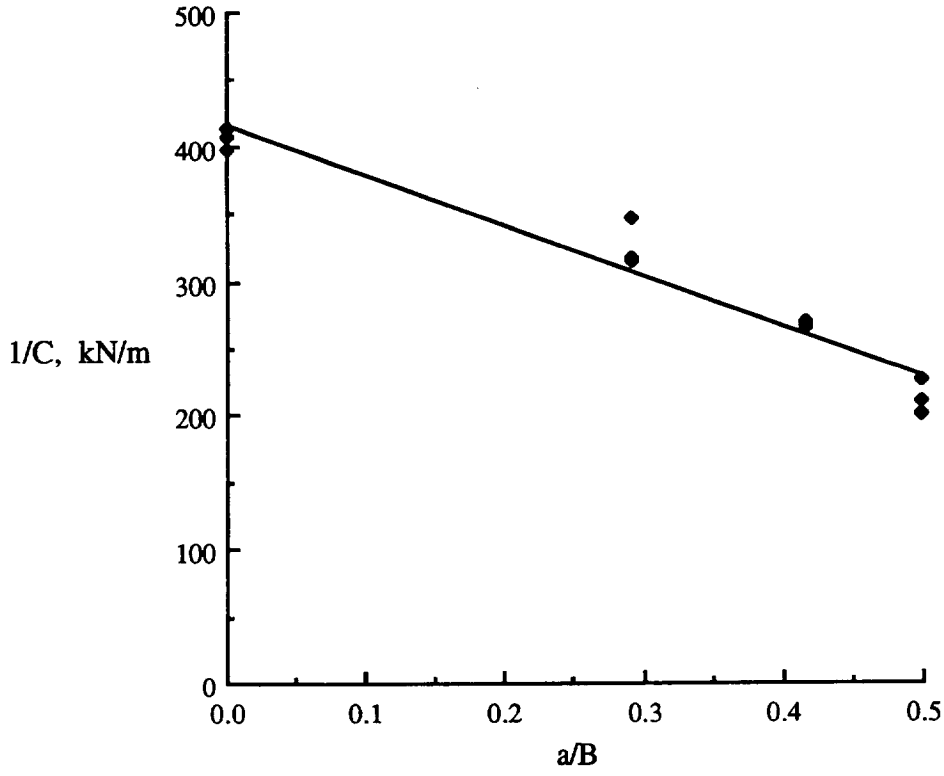

Figure 5. Variation of inverse of compliance 1/C versus nornalized delamination length a/B for the ECT specimens.

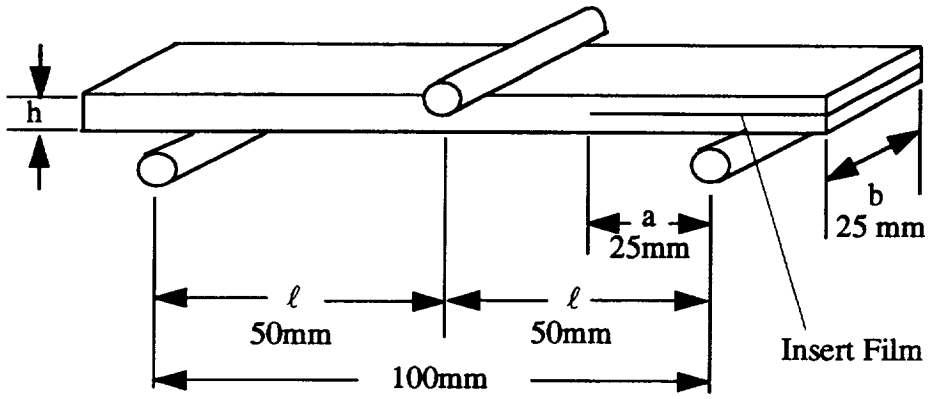

(a) ENF Test Specimen

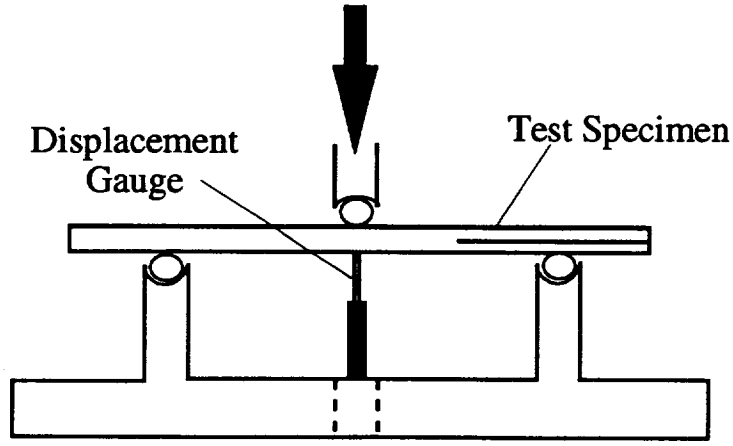

(b) ENF Test Apparatus

Figure 6. ENF test specimen and ENF test apparatus.

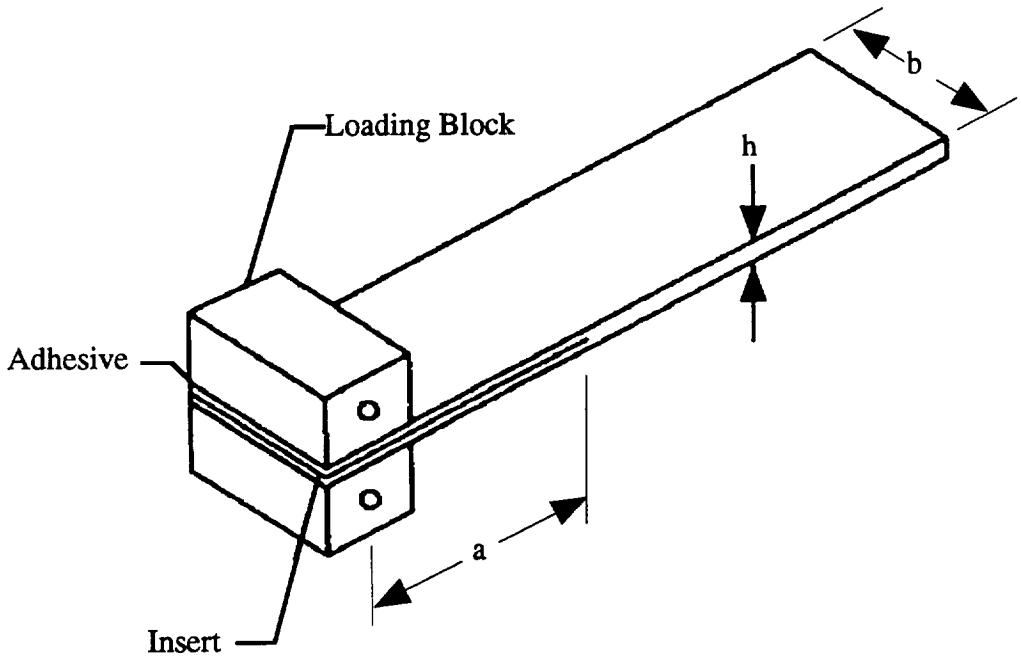

Figure 7. Schematic of the DCB specimen.

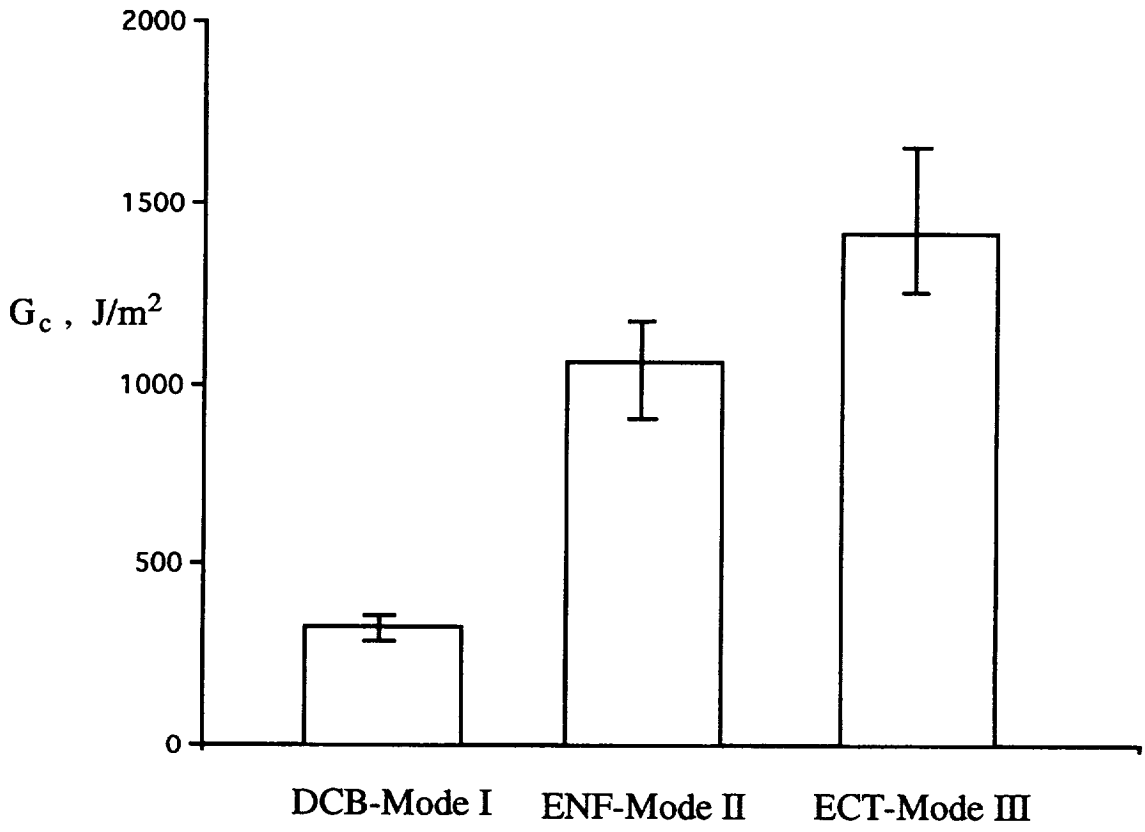

Figure 8. Comparison of various modes of fracture toughness for G40-800/R6376 graphite/epoxy laminates.

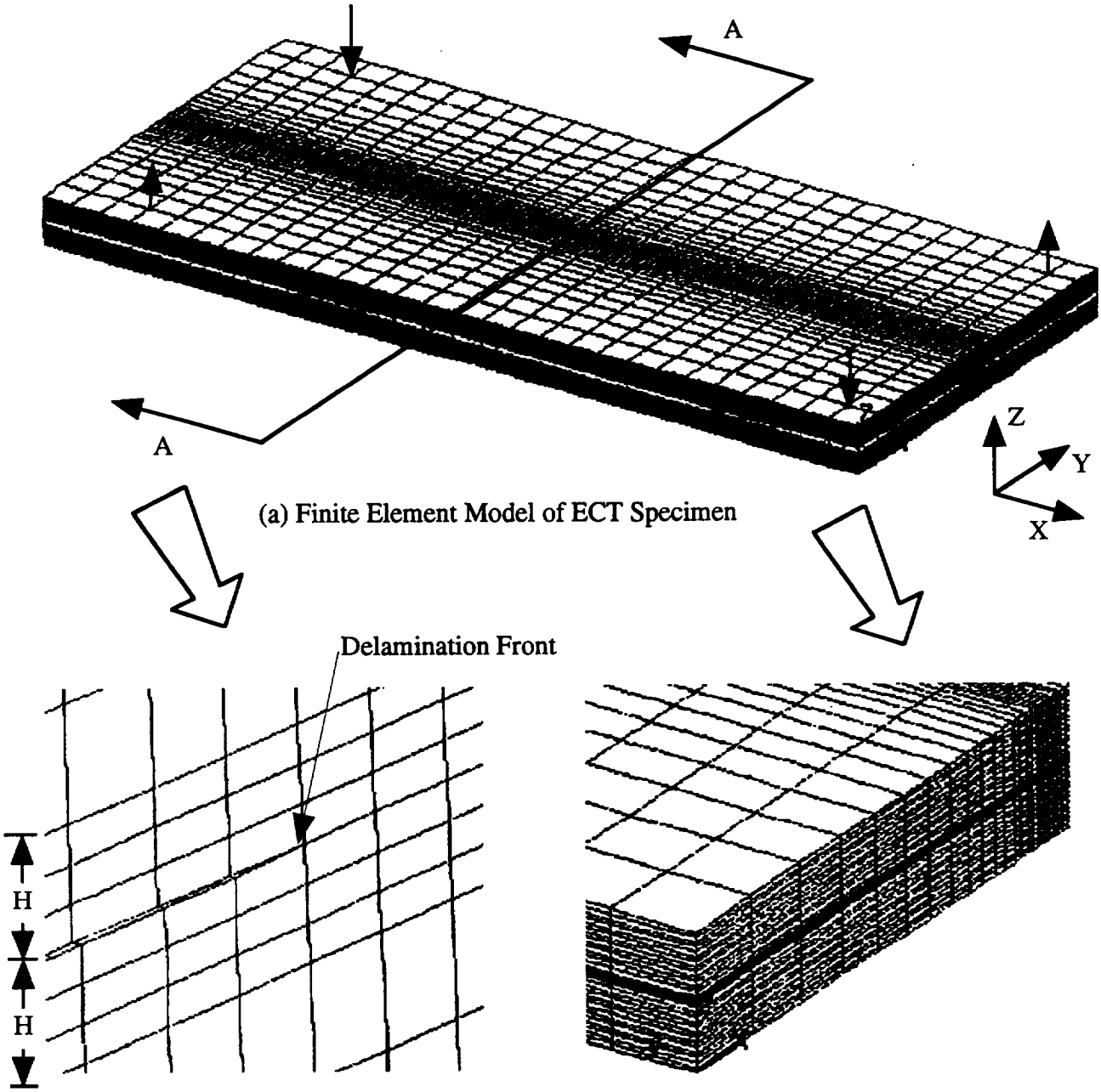

(a) Finite Element Model of ECT Specimen

(b) Details of Modeling near the Crack Front on Section A-A

(c) Details of Modeling near a Corner

Figure 9. Three-dimensional finite elemet eodel for ECT specimen C5.

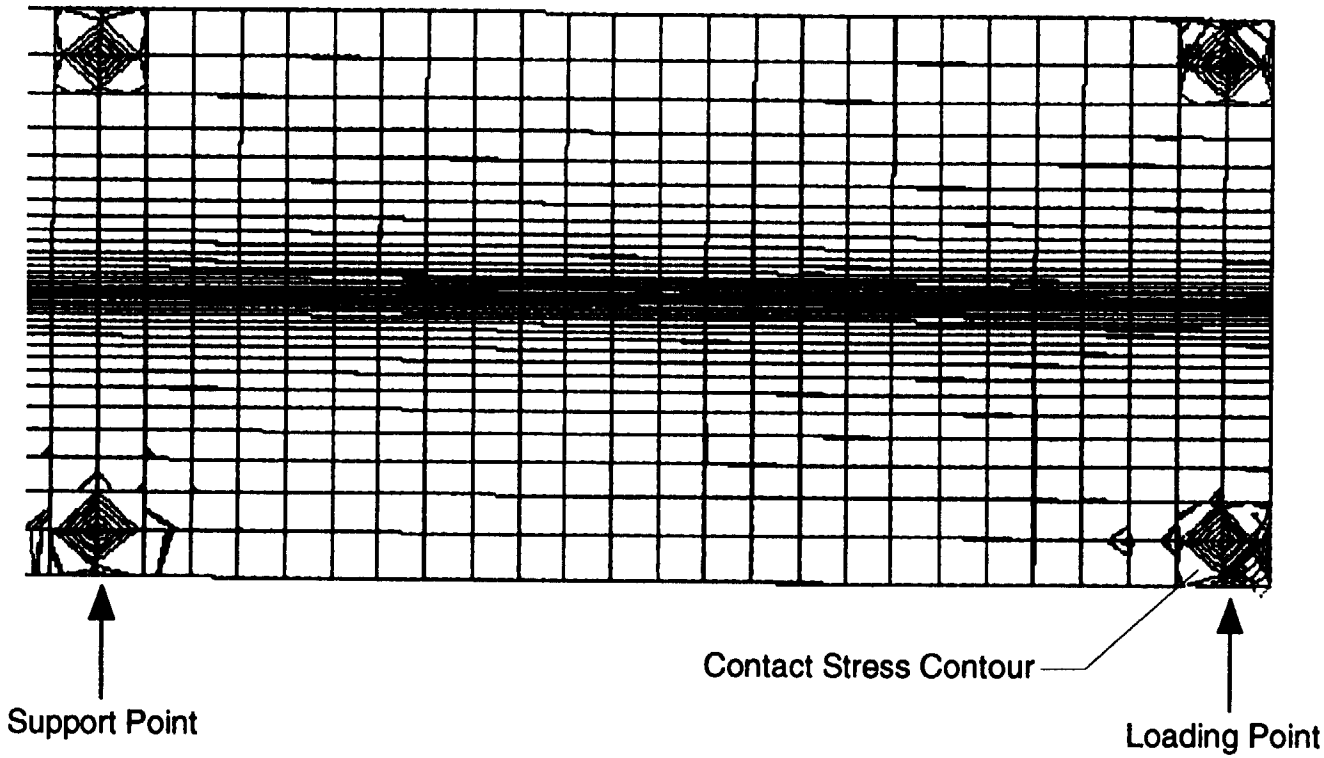

Figure 10. Contact stress distribution at the mid-plane for ECT specimen C5.

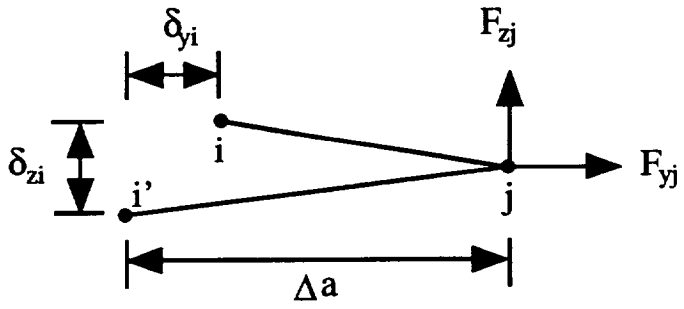

(a) Two-Dimensional Case

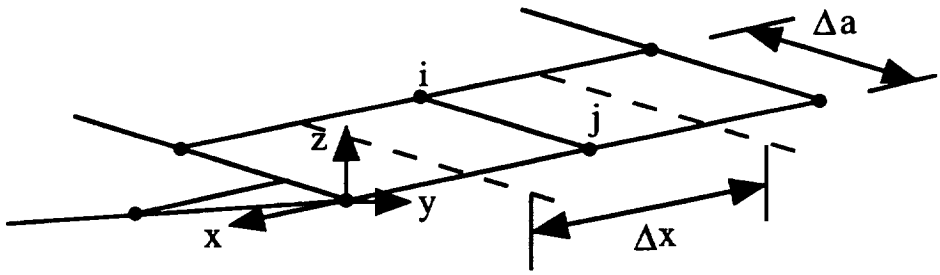

(b) Three-Dimensional Case

Figure 11. VCCT for two-dimensional four-node elements and three-dimensional eight-node solid elements.

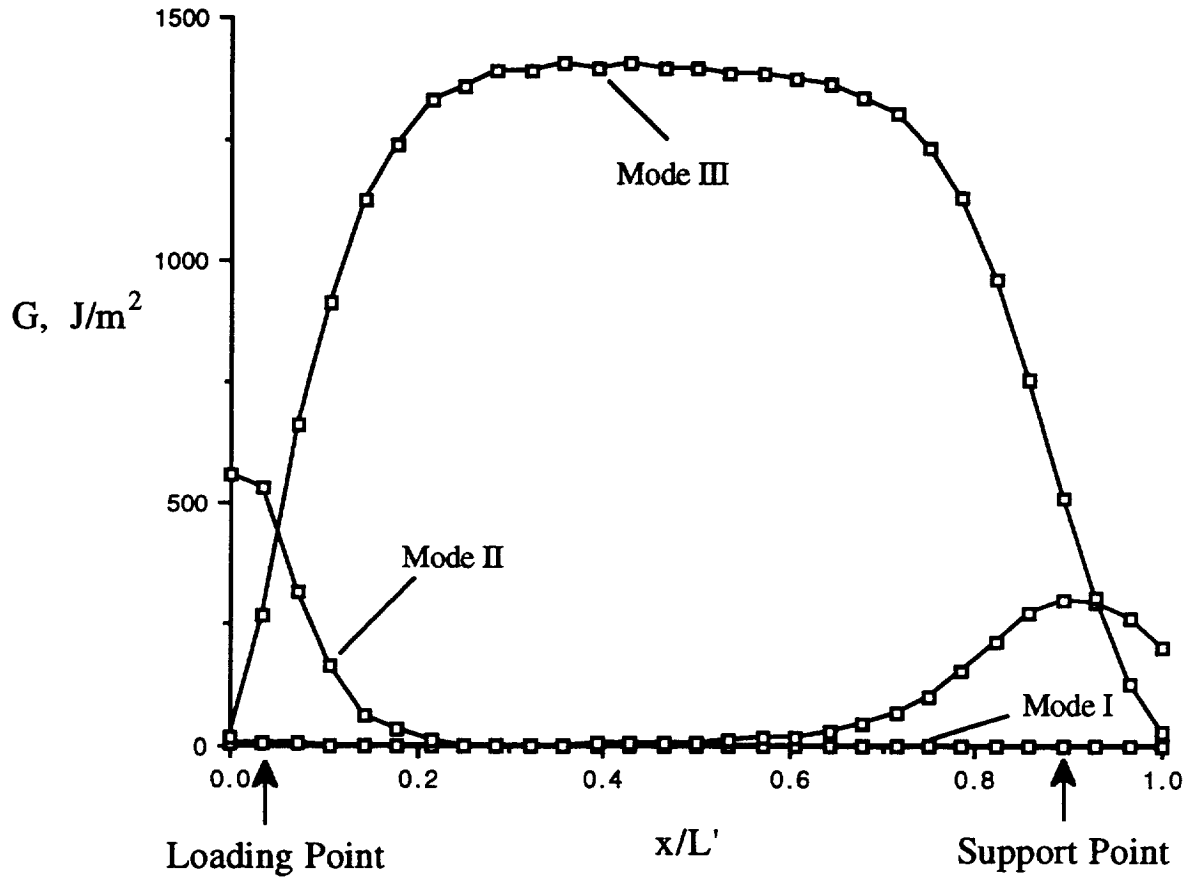

Figure 12. Distribution of strain energy release rate components along the delamination front for specimen C5 at (ã/B)=0.5.

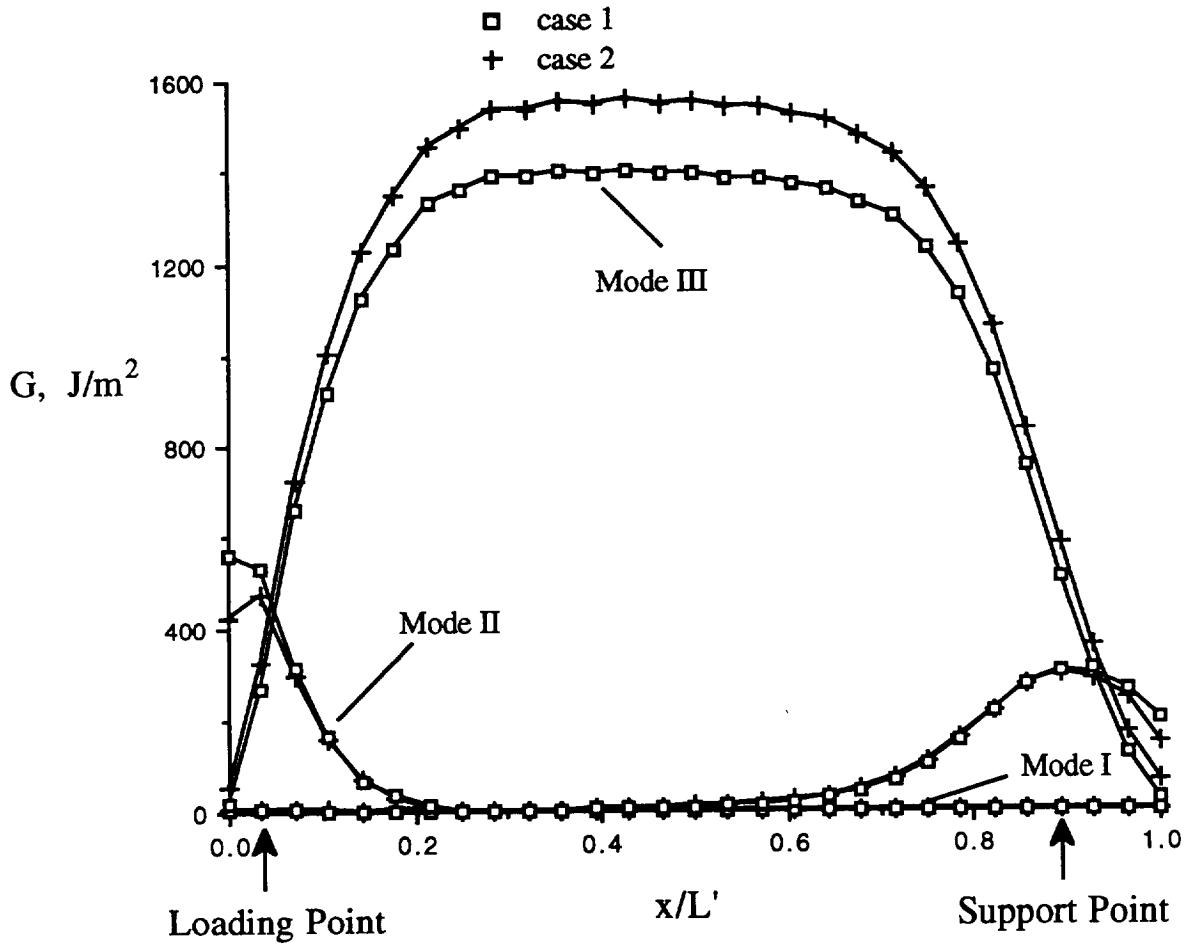

Figure 13. Comparison of strain energy release rate components along the delamination front for different shear modulus G_{23}.

REPORT DOCUMENTATION PAGE

Form Approved
OMB No. 0704-0188

1. AGENCY USE ONLY *(Leave blank)*	2. REPORT DATE	3. REPORT TYPE AND DATES COVERED
	August1996	Technical Memorandum

4. TITLE AND SUBTITLE

Evaluation of the Edge Crack Torsion (ECT) Test for Mode III Interlaminar Fracture Tougness of Laminated Composites

5. FUNDING NUMBERS

WU 505-63-50-04

6. AUTHOR(S)

Jian Li, Shaw Ming Lee, Edward W. Lee, and T. Kevin O'Brien

7. PERFORMING ORGANIZATION NAME(S) AND ADDRESS(ES)

NASA Langley Research Center
Hampton, VA 23681-0001 and
Vehicle Structures Directorate
U.S. Army Research Laboratory
NASA Langley Research Center, Hampton, VA 23681-0001

8. PERFORMING ORGANIZATION REPORT NUMBER

9. SPONSORING/MONITORING AGENCY NAME(S) AND ADDRESS(ES)

National Aeronautics and Space Administration
Washington, DC 20546-0001 and
U.S. Army Research Laboratory
Adelphi, MD 20783-1145

10. SPONSORING/MONITORING AGENCY REPORT NUMBER

NASA TM-110264
ARL-TR-1210

11. SUPPLEMENTARY NOTES

Li: NRC, Langley Research Center, Hampton, VA; Lee: Hexcel Composites, Anaheim, CA; Lee: Bell Helicopter Textron, Fort Worth, TX; O'Brien: Langley Research Center, Hampton, VA. Presented at the ASTM 13th Symposium on Composite Materials: Testing and Design, May 1996, Orlando, FL.

12a. DISTRIBUTION/AVAILABILITY STATEMENT

Unclassified - Unlimited

Subject Category 24

12b. DISTRIBUTION CODE

13. ABSTRACT *(Maximum 200 words)*

An analytical and experimental investigation was carried out on G40-800/R6376 graphite epoxy laminates to evaluate the Edge Crack Torsion (ECT) test as a candidate for a standard Mode III interlaminar fracture toughness test for laminated composites. The ECT test consists of a $[90/(\pm 45)_3/(\mp 45)_3/90]_S$ laminate with a delamination introduced by a non-adhesive film at the mid-plane along one edge and loaded in a special fixture to create torsion along the length of the laminate. Dye penetrate enhanced X-radiograph of failed specimens revealed that the delamination initiated at the middle of the specimen length and propagated in a self similar manner along the laminate mid-plane. A three-dimensional finite element analysis was performed that indicated that a pure Mode III delamination exists at the middle of specimen length away from both ends. At the ends near the loading point a small Mode II component exists. However, the magnitude of this Mode II strain energy release rate at the loading point is small compared to the magnitude of Mode III component in the mid-section of the specimen. Hence, the ECT test yielded the desired Mode III delamination. The Mode III fracture toughness was obtained from a compliance calibration method and was in good agreement with the finite element results. Mode II End-Notched Flexure (ENF) tests and Mode I Double Cantilever Beam (DCB) tests were also performed for the same composite material. The Mode I fracture toughness was much smaller than both the Mode II and Mode III fracture toughness. The Mode II fracture toughness was found to be 75% of the Mode III fracture toughness.

14. SUBJECT TERMS

Composite materials; Fracture tougness; Delamination; Compliance calibration; Three-dimensional finite element analysis; Strain energy release rate

15. NUMBER OF PAGES

34

16. PRICE CODE

A03

17. SECURITY CLASSIFICATION OF REPORT	18. SECURITY CLASSIFICATION OF THIS PAGE	19. SECURITY CLASSIFICATION OF ABSTRACT	20. LIMITATION OF ABSTRACT
Unclassified	Unclassified		